

This is an Open Access document downloaded from ORCA, Cardiff University's institutional repository: <https://orca.cardiff.ac.uk/id/eprint/152458/>

This is the author's version of a work that was submitted to / accepted for publication.

Citation for final published version:

Hayakawa, Akihiro, Hayashi, Masao, Kovaleva, Marina , Gotama, Gabriel J., Okafor, Ekenechukwu C., Colson, Sophie, Mashruk, Syed, Valera Medina, Agustin , Kudo, Taku and Kobayashi, Hideaki 2023. Experimental and numerical study of product gas and N₂O emission characteristics of ammonia/hydrogen/air premixed laminar flames stabilized in a stagnation flow. Proceedings of the Combustion Institute 39 (2) , pp. 1625-1633. 10.1016/j.proci.2022.08.124

Publishers page: <https://doi.org/10.1016/j.proci.2022.08.124>

Please note:

Changes made as a result of publishing processes such as copy-editing, formatting and page numbers may not be reflected in this version. For the definitive version of this publication, please refer to the published source. You are advised to consult the publisher's version if you wish to cite this paper.

This version is being made available in accordance with publisher policies. See <http://orca.cf.ac.uk/policies.html> for usage policies. Copyright and moral rights for publications made available in ORCA are retained by the copyright holders.



Experimental and numerical study of product gas and N₂O emission characteristics of ammonia/hydrogen/air premixed laminar flames stabilized in a stagnation flow

Akihiro Hayakawa^{a,*}, Masao Hayashi^{a,b}, Marina Kovaleva^c,
Gabriel J. Gotama^a, Ekenechukwu C. Okafor^d, Sophie Colson^a,
Syed Mashruk^c, Agustin Valera-Medina^c, Taku Kudo^a, Hideaki Kobayashi^a

^a*Institute of Fluid Science, Tohoku University, 2-1-1 Katahira, Aoba-ku, Sendai 980-8577, Japan*

^b*Department of Aerospace Engineering, Tohoku University, Aramaki, Aoba-ku, Sendai 980-8579, Japan*

^c*College of Physical Sciences and Engineering, Cardiff University, Queen's building, Cardiff CF24 3AA, United Kingdom*

^d*Department of Mechanical Engineering, Kyushu University, 744 Motoooka, Nishi-ku, Fukuoka 819-0395, Japan*

Abstract

In order to achieve carbon neutrality, the use of ammonia as a fuel for power generation is highly anticipated. The utilization of a binary fuel consisting of ammonia and hydrogen can address the weak flame characteristics of ammonia. In this study, the product gas characteristics of ammonia/hydrogen/air premixed laminar flames stabilized in a stagnation burner were experimentally and numerically investigated for various equivalence ratios for the first time. A trade-off relationship between NO and unburnt ammonia was observed at slightly rich conditions. At lean conditions, NO reached a maximum value of 8,700 ppm, which was larger than that of pure ammonia/air flames. The mole fraction of nitrous oxide (N₂O) which has large global warming potential rapidly increased around the equivalence ratio of 0.6, which was attributed to the effect of a decrease in flame temperature downstream of the reaction zone owing to heat loss to the stagnation wall. To understand this effect further, numerical simulations of ammonia/hydrogen/air flames were conducted using the stagnation flame model for various equivalence ratios and stagnation wall temperatures. The results show that the important reactions for N₂O production and reductions are $\text{NH} + \text{NO} = \text{N}_2\text{O} + \text{H}$, $\text{N}_2\text{O} + \text{H} = \text{N}_2 + \text{OH}$, and $\text{N}_2\text{O} (+\text{M}) = \text{N}_2 + \text{O} (+\text{M})$. A decrease in flame temperature in the post flame region inhibited N₂O reduction through $\text{N}_2\text{O} (+\text{M}) = \text{N}_2 + \text{O} (+\text{M})$ because this reaction has a large temperature dependence, and thus N₂O was detected as a product gas. N₂O is reduced through $\text{N}_2\text{O} (+\text{M}) = \text{N}_2 + \text{O} (+\text{M})$ in the post flame region if the stagnation wall temperature is sufficiently high. On the other hand, it was clarified that an increase in equivalence ratio enhances H radical production and promotes N₂O reduction by H radicals through the reaction of $\text{N}_2\text{O} + \text{H} = \text{N}_2 + \text{OH}$.

Keywords: Ammonia; Hydrogen; Product gas; Stagnation flame; Nitrous oxide

*Corresponding author.

1. Introduction

In an effort to achieve neutrality, the utilization of ammonia not only as hydrogen energy carrier but also as a carbon-free fuel is anticipated. Recently, many studies regarding fundamental combustion characteristics of ammonia have been carried out [1,2]. Research has found that to apply ammonia as a fuel for power generation, there are mainly two challenges: weak flame characteristics and product gas characteristics. Power generation in a gas turbine with ammonia as the sole fuel was successfully demonstrated by the group of AIST and Tohoku University in 2015 [3]. In this gas turbine system, flame enhancement using a heat-regenerative system was employed. Thus, it was found that flame enhancement is important to stabilize an ammonia flame in a power generation system.

Co-firing with another fuel is a promising solution to improve the flame intensity and stability of ammonia. Since ammonia also acts as a hydrogen energy carrier and hydrogen can be obtained using an on-board hydrogen generating device as demonstrated by SI engine studies [4,5], co-firing with hydrogen is an attractive option. Furthermore, Khateeb et al. [6] studied flame characteristics of ammonia/hydrogen blends in a swirl combustor. Fundamental studies of ammonia/hydrogen flames have been performed by many researchers, including the measurement of laminar burning velocity and Markstein length [7-9]. Ichikawa et al. [8] studied ammonia/hydrogen/air flames for various hydrogen fractions at stoichiometry and showed that the value of the laminar burning velocity increased exponentially as the volumetric fraction of hydrogen in the binary fuel increased.

Understanding product gas characteristics is another important challenge, the study of which is necessary to satisfy emissions regulations. Due to the very low laminar burning velocity of an ammonia/air flames, it is difficult to stabilize ammonia/air flame in a nozzle burner. However, Brackmann et al. succeed in stabilizing ammonia/air flames using the stagnation flame configuration, allowing for the study of flame characteristics using laser diagnostics [10]. Hayakawa et al. [11] applied the stagnation flame configuration to evaluate the product gas characteristics of ammonia/air premixed laminar flames, and the product gas characteristics, such as NO and unburnt ammonia. This study clarified that there is a trade-off behavior between NO and unburnt ammonia emissions. The research group at Tohoku University developed the rich-lean two-stage flame concept to reduce NO and unburnt ammonia simultaneously based on these trade-off characteristics [12]. The concept has been applied in an actual gas turbine combustor at AIST and succeeded in reducing the NOx emission [13].

Recently, product gas characteristics of ammonia/hydrogen/air flames in a swirl combustor were studied for various equivalence ratio conditions by Mashruk et al. [14]. The interesting point in this

study is that nitrous oxide (N_2O) was detected at lean and rich conditions. Since the global warming potential of N_2O is almost 300 times that of CO_2 over a period of 100 years [15], not only NO and unburnt ammonia, but also N_2O emissions should be reduced as much as possible. A study of turbulent, swirl stabilized, ammonia/air flames by Okafor et al. [16] identified that heat loss promotes N_2O emissions. However, because of complicated flow structure in a swirl combustor, it is difficult to discuss the production and reduction mechanism of N_2O , and this study is not available for chemistry validation.

Based on this background, the objective of this study is to clarify the product gas characteristics of ammonia/hydrogen/air premixed laminar flames stabilized in a stagnation flow for the first time. In addition, N_2O emissions were also observed in this configuration, as discussed in Section 3.1. Another objective is to clarify the production/reduction mechanisms of N_2O using numerical simulation with detailed reaction chemistry.

2. Experimental and numerical setup

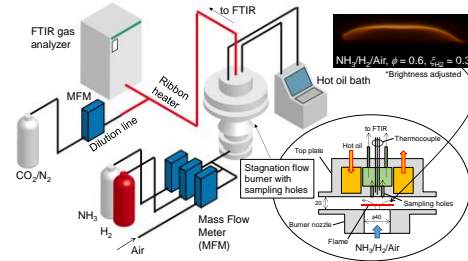


Fig. 1. Schematic figure of the experimental setup and the burner structure used in this study.

Figure 1 shows the schematic of the experimental setup, with a burner structure identical to that employed in a previous study by Hayakawa et al. [11]. NH_3 and H_2 were used for the fuel blend and dry air was used as the oxidizer. Mass flow meters (Kofloc, 3760, accuracy 1.0%FS, for NH_3 and H_2 , and Kofloc 3765, accuracy 1.5%FS, for Air) measured the flow rate, which was controlled by needle valves. The hydrogen fraction in the binary fuel of ammonia/hydrogen, ξ_{H_2} , was defined by Eq. (1) [8],

$$\xi_{H_2} = \frac{[H_2]}{[NH_3] + [H_2]}, \quad (1)$$

where $[X]$ represents mole fraction of species X . In this study, the hydrogen fraction in the binary fuel was set to $\xi_{H_2} = 0.3$. All the experiments were conducted under atmospheric pressure. The equivalence ratio, ϕ , was varied from 0.57 to 1.4. To stabilize the flame for various equivalence ratio conditions, the mixture inlet velocity, U_{in} , was adjusted depending on the equivalence ratio. The mixture inlet temperature remained constant at $295 \text{ K} \pm 2 \text{ K}$ for all conditions. The mixture was supplied to a nozzle burner with a

burner outlet diameter of 40 mm. To generate a stagnation flow, a top plate was mounted 20 mm above the burner outlet. Sampling holes were located in the top plate, allowing for the product gas to be drawn through the holes. The plate temperature was controlled by a hot oil bath circulating silicone oil. As shown in Fig. 1, an almost flat flame could be stabilized in the stagnation flow for various equivalence ratio conditions. Three thermocouples were inserted inside the top plate at different depths, staggered 1 mm apart. By extrapolating the temperature measured by these thermocouples, the surface temperature of the top plate, T_w , could be estimated. Values of U_{in} and T_w at experimental conditions were provided in the supplementary material. Reynolds number based on the burner outlet diameter was 1,083 for the fastest mixture inlet velocity condition, and thus the flow remained laminar.

The product gas was analyzed by a FTIR (Fourier Transform Infrared) gas analyzer combined with oxygen and hydrogen analyzers (Best Instruments Co. Ltd., BOB-2000FT), with a measurement uncertainty of 2% of the full measurement range. The gas sampling lines were heated to prevent the condensation of water vapor in the product gas. Under some experimental conditions, the gas concentration exceeded the measurement range for the FTIR gas analyzer. In addition, to stabilize weak ammonia-based flames, a reduction of the product gas sampling rate was necessary. In this study, the dilution sampling method [17] was employed for this purpose. A CO_2/N_2 mixture gas ($\text{CO}_2 = 15.9\%$ vol.) was employed as the dilution gas, with CO_2 used as the tracer species of the dilution sampling method. Instead of measuring the actual flow rate of the sampled gas, the dilution ratio, as well as the actual mole fraction of the species of interest could be calculated from the measured value of the tracer species (CO_2) by the FTIR gas analyzer. Further details of the dilution sampling method could be found elsewhere [17].

To understand the detailed structure and chemistry of the flame, one-dimensional numerical simulations were carried out using CHEMKIN-PRO [18] software. To simulate freely propagating flames and stagnation flames, the Premixed Laminar Flame-Speed Calculation model and the Premixed Laminar Burner-Stabilized Stagnation Flame model were employed, respectively. For the reaction chemistry, detailed reaction mechanisms developed by Gotama et al. [9], Okafor et al [19], Nakamura et al. [20, 21], Otomo et al. [22], Stagni et al [23], and Zhang et al. [24] were employed. For the numerical simulation of stagnation flames, wall temperature and mixture inlet velocity values were required and were obtained using 6th order polynomial fitting on the experimental data. Further details can be found in the supplementary material.

3. Results and discussions

3.1 Experimental results

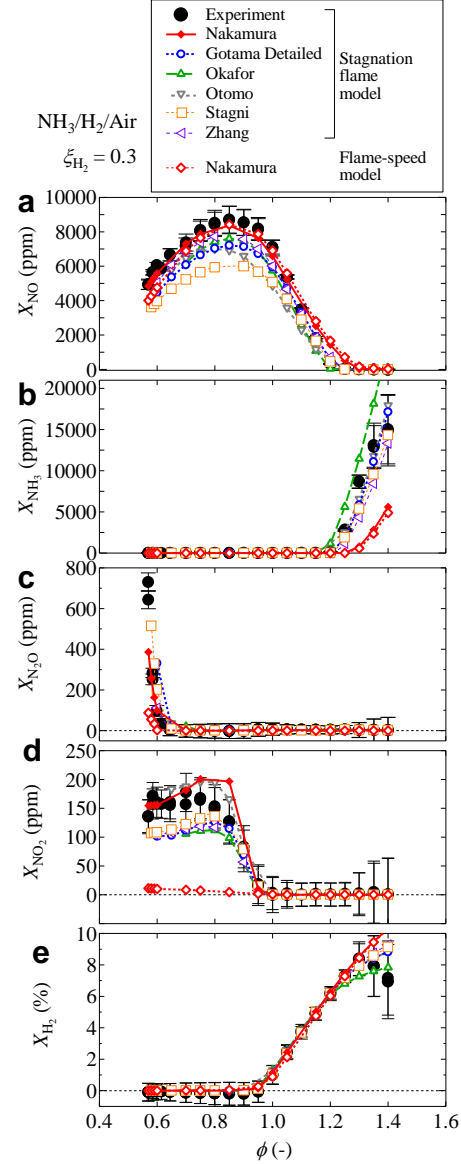


Fig. 2. Relationship between the mole fractions of (a) NO, (b) NH_3 , (c) N_2O , (d) NO_2 , and (e) H_2 and the equivalence ratio, ϕ . The numerical results calculated using Gotama mech [9], Okafor mech [19], Nakamura mech [20, 21] and Otomo mech [22], Stagni mech [23], and Zhang mech [24] were also plotted.

Figure 2 shows the relationship between the mole fraction of species i , X_i , and equivalence ratio, ϕ . Values of the mole fraction from the numerical stagnation flame model was taken at the end point of the computational domain, which corresponds to the stagnation plate location. The maximum NO mole

fraction was about 8,700 ppm for $\phi \sim 0.85$, as shown in Fig. 2a, with a decrease in NO at either side of the peak. Since the maximum NO mole fraction of pure ammonia/air flames was approximately 3,500 ppm in the same flame configuration [11], this shows the effect of increasing hydrogen fraction on NO. A trade-off behavior between X_{NO} and X_{NH_3} was observed, resulting in only a narrow window in the rich region where the mole fractions of these species are simultaneously low. Such equivalence ratio is termed as the optimal equivalence ratio, which was about $\phi \sim 1.20$ for this mixture. This optimal equivalence ratio is also the target equivalence ratio of the primary zone in the rich-lean two-stage combustion concept to achieve simultaneous reduction of NO and unburnt ammonia at the combustor exit [12]. In the pure ammonia/air case, the optimal equivalence ratio was approximately 1.07 [11], hence the optimal equivalence ratio shifted to the rich side with the addition of hydrogen in the fuel.

In ammonia/hydrogen/air premixed laminar flames, the value of X_{NO_2} increased in the lean region, and the maximum value within the conditions tested in the present study was found to be approximately 150 ppm, as shown in Fig. 2d. Also, the value of X_{H_2} increased up to $\sim 8\%$ in the rich region.

Of particular significance is the emission of N_2O which rapidly increased at an equivalence ratio of around 0.6 and the value of X_{N_2O} reached a maximum value of ~ 700 ppm within the experimental conditions tested in this study. To reduce greenhouse gas emissions, it is relevant to clarify the underlying behavior of N_2O production in ammonia/hydrogen/air flames.

Results of numerical simulations are given in Fig. 2. The numerical results obtained from the stagnation flame simulations agree well with the experimental results. Especially for N_2O characteristics, results obtained using Nakamura mech, Gotama mech and Stagni mech were close to the experimental results. However, the results of NO obtained using Gotama mech and Stagni mech slightly lower than the experimental value. For the lean condition, the results obtained by the Nakamura mechanism were especially close to the experimental results. Thus, further discussion of N_2O production/reduction mechanisms will be based on the results obtained using Nakamura mech.

Product gas characteristics of freely propagating flames obtained using Nakamura mech are also plotted in Fig. 2. Since the computational domain of the freely propagating flame was longer than the stagnation flame domain, the freely propagating flame mole fraction sampling point was adjusted to be a set distance downstream from the peak heat release rate value. This distance was calibrated to the distance between the stagnation flame peak heat release rate value and the stagnation wall, Δ . The mole fraction of NO_2 for the freely propagating flame was lower than that for the stagnation flame. A slight increase in N_2O around ϕ of 0.6 was also observed in the case of the

freely propagating flame. The trends for other species were similar with the stagnation flames.

Figure 3 gives a comparison between the structure of the stagnation and the freely propagating flames of ammonia/hydrogen/air mixtures. The position of the peak heat release rate was shifted to 0 mm for all the flames. Because of the influence of the stagnation wall, the temperature in the post flame zone of the stagnation flame decreased closer to the wall. The mole fraction of NO rapidly increased in the flame region, showing a trend typical of fuel NO formation. For both types of flame, mole fraction of N_2O increased and decreased rapidly in the reaction zone for $\phi = 1.0$ and 1.2. For the stagnation flame at $\phi = 0.6$, N_2O mole fraction decreased gradually without ever reaching 0 ppm and maintained a constant value in the post flame (from ~ 5 mm onwards). However, for the case of freely propagating flame, the mole fraction of N_2O decreased to almost zero at around 6.5 mm.

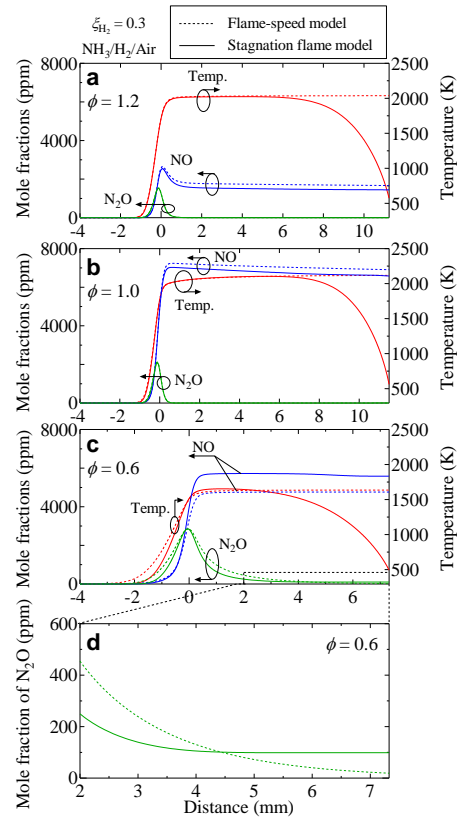


Fig. 3. Flame structure of $NH_3/H_2/Air$ flames at the equivalence ratios of (a) 1.2, (b) 1.0, and (c) 0.6. (d) represents the magnified view of N_2O mole fraction for downstream of (c).

To understand this N_2O behavior, a detailed analysis of N_2O production and reduction mechanisms are discussed below. First, important reactions for N_2O were identified.

Figure 4 shows the sensitivities for N_2O at the end point of the computational domain of $\text{NH}_3/\text{H}_2/\text{air}$ stagnation flames. In addition, to evaluate the contribution of elementary reactions to the production or reduction of N_2O , the integrated values of the production rate, I_R , were evaluated, and are shown in Fig. 5. Here, the value of I_R , was defined as Eq. (2),

$$I_R = \int_0^L \dot{\omega}_{R,i} dx, \quad (2)$$

where $\dot{\omega}_{R,i}$ is the rate of production of the species, i , through the reaction, R . The length of the integration domain, L , for the freely propagating flame was from the inlet to Δ downstream from the peak heat release rate, while that for the stagnation flame was from the inlet to the stagnation wall ($= 20 \text{ mm}$).

In the Nakamura mech, there are 18 elementary reactions that include N_2O in their equations. According to the results given in Figs. 4 and 5, the reactions R43, R46, R47, and R49 were considered to be the most important reactions for N_2O production, as summarized in Table 1. Note that the value of $I_{R46} + I_{R47}$ was presented in Fig. 5 because these reactions are duplicated. The values of I_{R46} and I_{R47} at $\xi_{\text{H}_2} = 0.3$ and $\phi = 0.6$ were $-1.73 \times 10^{-8} \text{ mol/cm}^2\text{s}$ and $-3.89 \times 10^{-6} \text{ mol/cm}^2\text{s}$, respectively, thus I_{R47} was dominant. Previous work explained the importance of R43 in the production of N_2O , and also R46 + R47 in the consumption of N_2O [25], and the same behavior is seen in $\text{NH}_3/\text{H}_2/\text{air}$ flames.

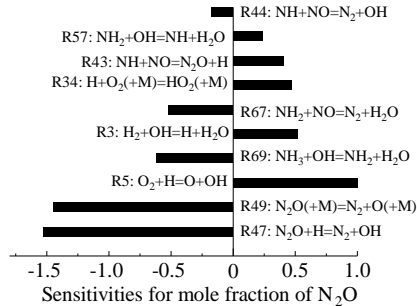


Fig. 4. Sensitivities for the mole fraction of N_2O at the endpoint of computational domain of $\text{NH}_3/\text{H}_2/\text{air}$ premixed stagnation flames at $\phi = 0.6$ and $\xi_{\text{H}_2} = 0.3$.

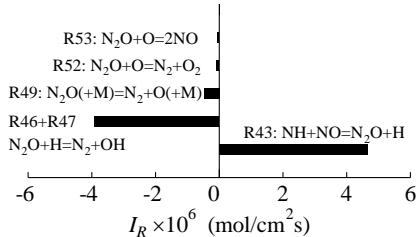


Fig. 5. I_R values regarding N_2O production/consumption reactions of $\text{NH}_3/\text{H}_2/\text{air}$ premixed stagnation flames at $\phi = 0.6$ and $\xi_{\text{H}_2} = 0.3$.

Table 1

Important reactions for N_2O production and consumption in Nakamura mech [20, 21]. The units are (cm, mol, s, cal).

No.	Reaction	A	n	E
43	$\text{NH} + \text{NO} = \text{N}_2\text{O} + \text{H}$	$1.80\text{E}+14$	-0.351	-244
46*	$\text{N}_2\text{O} + \text{H} = \text{N}_2 + \text{OH}$	$3.31\text{E}+10$	0	5,090
47*	$\text{N}_2\text{O} + \text{H} = \text{N}_2 + \text{OH}$	$7.83\text{E}+14$	0	19,390
49	$\text{N}_2\text{O} (+\text{M}) = \text{N}_2 + \text{O} (+\text{M})$	$9.90\text{E}+10$	0	57,960
	LOW	$6.62\text{E}+14$	0	57,500
$\text{O}_2/1.4/ \text{N}_2/1.7/ \text{H}_2\text{O}/12.0/ \text{NO}/3.0/ \text{N}_2\text{O}/3.5/$				

* Duplicated reactions

As shown in Table 1, R49 has large temperature dependence because of its large activation energy, while R43 has a small temperature dependence. It is also noted that the R43 competes for N_2 formation through R44, though this reaction also has a small temperature dependence ($n = -0.23$, $E = 0 \text{ cal/mol}$):

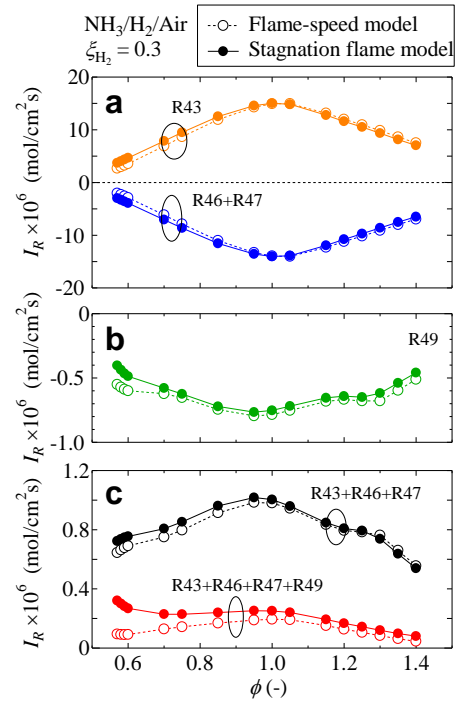
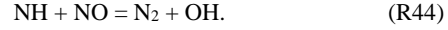


Fig. 6. Variation of I_R with equivalence ratio, ϕ (a) I_R values for each reactions; (b) I_R values of $I_{R43+R46+R47}$ and $I_{R43+R46+R47+R49}$ which corresponds to major N_2O production rate through the computational domain.

Figure 6 shows the variation in the integral production rate, I_R , with equivalence ratio, ϕ , for both freely propagating and stagnation flame simulations. Here, plotted condition corresponded to the numerical condition that the converged results could be obtained. As shown in Fig. 6a, the orders of I_{R43} and $I_{R46+R47}$ were larger by almost 10 times compared to the value

of I_{R49} . Since the orders of I_{R43} and $I_{R46+R47}$ are close, the order of $I_{R43+R46+R47}$ becomes close to that of I_{R49} , and the reaction of R49 becomes important. As shown in Fig. 6b, the values of $I_{R43+R46+R47+R49}$ increased slightly at around $\phi \sim 0.6$, as supported by Fig. 2c. In Fig. 2c, N_2O mole fraction of the freely propagating flame also increased slightly. However, this trend cannot be solely explained from the standpoint of I_R analysis in Fig. 6.

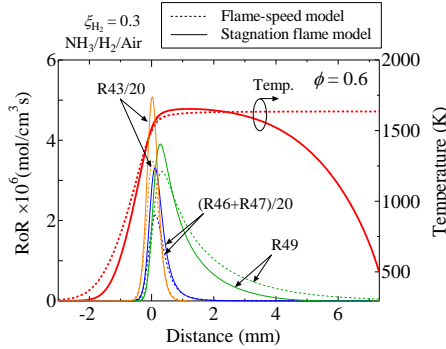


Fig. 7. Rate of Reaction (RoR) of $NH_3/H_2/Air$ for $\phi = 0.6$.

Figure 7 shows the rate of reaction (RoR) profiles of key reactions at $\phi = 0.6$ for N_2O production and consumption. The reaction rates of R43 and R46+R47 were larger than that of R49, and these reactions were found to occur only in the reaction zone. As for R49, although the peak value was in the reaction zone, this reaction continued in the post flame region. This can explain the freely propagating flame behavior seen in Fig. 3c, with the mole fraction of N_2O rapidly decreasing in the reaction zone and then continuing the decrease at a slower rate in the post flame region. This is supported by Fig. 7, where the R49 reaction continues after 5 mm. On the other hand, for the stagnation flame, Fig. 3c shows that N_2O mole fraction reached a steady state after 5 mm, which can be linked to R49 reaching a zero reaction rate in the post flame region. Because of the low temperature of the stagnation wall, the temperature downstream of the flame decreased at different rates in the two flame configurations. As shown in Table 1, R49 has large temperature dependence. Thus, existence of low temperature region inhibited N_2O reduction through R49.

3.2 Effects of the stagnation wall temperature and equivalence ratio

To further understand this N_2O behavior, a numerical simulation of the stagnation flame for various stagnation wall temperatures was carried out focusing on a range of lean equivalence ratio conditions. In the numerical simulation in this section, the mixture inlet velocity was set to 25.5 cm/s for all simulations, which is the same as the inlet velocity at $\phi = 0.6$, given in figures listed in Section 3.1. The equivalence ratios were varied under constant

stagnation wall temperature conditions and vice versa, as shown in Fig. 8. Here, plotted condition corresponded to the numerical condition that the converged results could be obtained. Note that the 1654.3 K was equal to the adiabatic flame temperature at equilibrium of $NH_3/H_2/air$ flame for $\xi_{H_2} = 0.3$ and $\phi = 0.6$.

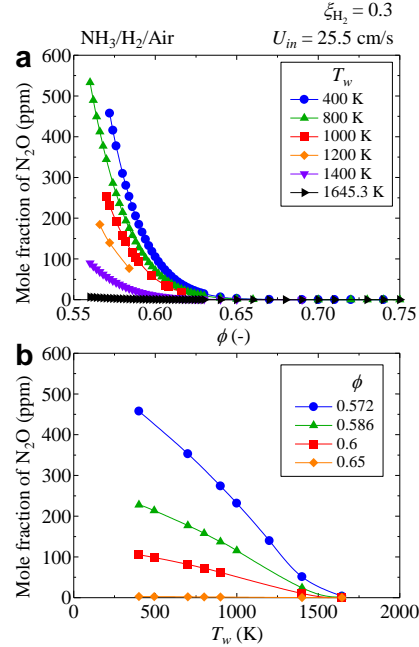


Fig. 8. Effects of (a) equivalence ratio, ϕ , and (b) stagnation wall temperature, T_w , on N_2O characteristics of $NH_3/H_2/Air$ flames.

The mole fraction of N_2O decreased with an increase in the equivalence ratio and stagnation wall temperature, such that N_2O production was almost zero for $\phi > 0.65$ or $T_w > 1645$ K. To understand this trend, important reactions for N_2O production were investigated in further detail.

Figure 9 shows the effect of equivalence ratio and stagnation wall temperature on the I_R values obtained from the rate of production of N_2O through the important reactions listed in Table 1. The change in I_R values for $\phi = 0.65$ were relatively small compared to other equivalence ratio conditions. For $\phi \leq 0.6$, with an increase in the stagnation wall temperature, the values of I_{R43} increased, and $I_{R46+R47}$ and I_{R49} decreased. As shown in Fig. 9d, the value of $I_{R43+R46+R47+R49}$ increased with a decrease in the stagnation wall temperature for $\phi \leq 0.6$. The change in $I_{R43+R46+R47+R49}$ at $\phi = 0.65$ was small compared to other equivalence ratio conditions, and this trend is similar with N_2O mole fraction shown in Fig. 8b.

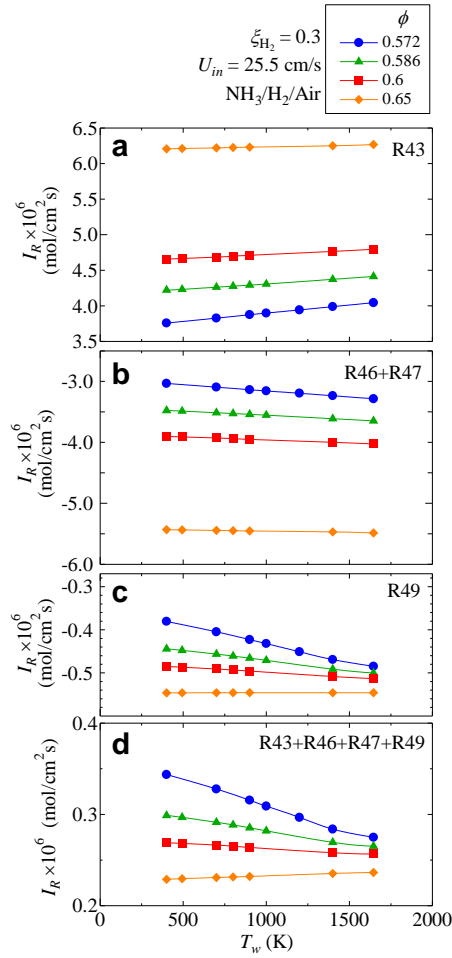


Fig. 9. Variation of I_R with stagnation wall temperature, T_w . (a) I_{R43} , (b) I_{R46+47} , (c) I_{R49} , and (d) $I_{R43+46+47+49}$.

To further understand the trend in I_R , the flame structure was investigated. Figure 10a showed the species profiles of H and N_2O and the temperature profile. Figure 10b shows the change in the maximum value of H and N_2O mole fractions within the computational domain. As shown in Fig. 10b, the change in the maximum value of N_2O was small compared to that of H, which increased with an increase in equivalence ratio. Since the major N_2O reduction occurs through R46+R47, N_2O reduction through R46+R47 was enhanced with an increase in the equivalence ratio. This corresponds to the decrease in $I_{R46+R47}$ (i.e., an increase in consumption rate) with an increase in the equivalence ratio shown in Fig. 9b. Although R47 also has large temperature dependence as shown in Table 1, R47 mainly occurs in flame region where N_2O and H exist. Thus, the influence on the low temperature region was considered to be small compared to R49. Therefore, it was considered that the decrease in N_2O with increasing equivalence ratio was caused by an

increase in H radical concentration. Figure 11 shows the I_R value of H and H_2 production reactions. H radical is mainly produced from H_2 , NH_2 , and NH , while H_2 is produced from NH_2 , HNO , and NH_3 . Therefore, the increase in H radical concentration with increasing equivalence ratio was caused by higher ammonia and hydrogen concentrations in the fuel/air mixture.

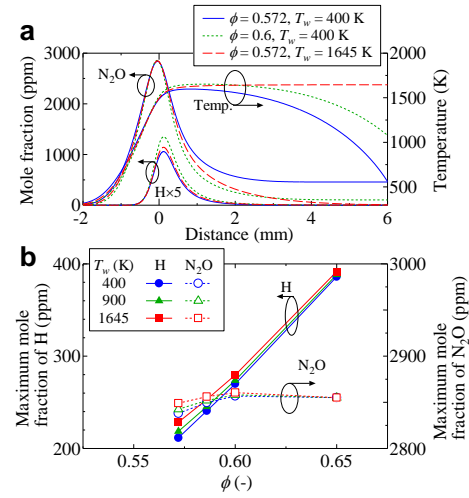


Fig. 10. (a) Flame structure and (b) the variations of maximum values of H and N_2O in the computational domain with equivalence ratio.

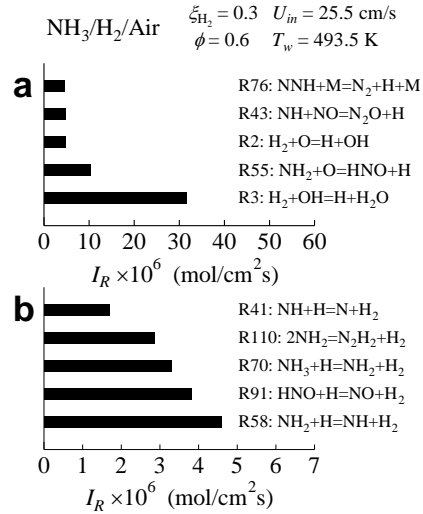


Fig. 11. I_R value of (a) H production and (b) H_2 production.

Even for very lean equivalence ratio cases, i.e., small H radical concentrations, if the stagnation wall temperature is sufficiently high, then N_2O can be reduced through the reaction of R49 in the post flame region as shown in the red dash curve in Fig. 10a. However, if the amount of H radical is not sufficient and the stagnation wall temperature is low, R46, R47 and R49 have less contribution in reducing N_2O . In

this case, as shown in the blue solid curve in Fig. 10a, in the post flame region, N_2O would not be reduced completely and therefore the N_2O content in the product gas rises.

In the actual combustor, such as a gas turbine or an internal combustion engine, the combustion occurs in a closed volume, and this configuration involves heat loss to the wall. Thus, to reduce N_2O emission near the low temperature region, the control of equivalence ratio is considered to be important.

4. Conclusions

To understand the product gas characteristics of ammonia/hydrogen/air flames, experimental and numerical studies were conducted for a binary fuel of ammonia and hydrogen. Premixed laminar flames were stabilized in a stagnation flow configuration, and the product gas was sampled through a stagnation flow-generating top plate. The following results were obtained in this study:

1. The maximum value of NO, within the range of conditions tested in this study was approximately 8,700 ppm, which is larger than the maximum NO measured in pure ammonia/air flames for the same configuration.
2. There is a trade-off between NO and unburnt ammonia emissions, leading to an equivalence ratio condition where both emissions are simultaneously low. This optimum low emission equivalence ratio, which was richer than that of pure ammonia/air flames, indicates that rich-lean two-stage combustion may be applicable for ammonia/hydrogen/air flames.
3. The mole fraction of N_2O rapidly increased as equivalence ratio decreased below 0.6. Because of heat loss to the stagnation wall, the temperature downstream of the flame in the stagnation flame configuration was lower than that in the freely propagating flame. Thus, the reduction of N_2O by $\text{N}_2\text{O} (+\text{M}) = \text{N}_2 + \text{O} (+\text{M})$ which has large temperature dependence was inhibited in the stagnation flame configuration, and N_2O could not be reduced completely.
4. With an increase in equivalence ratio, the H radical mole fraction increases. Thus, N_2O reduction is emphasized through the reaction of $\text{N}_2\text{O} + \text{H} = \text{N}_2 + \text{OH}$. If the mole fraction of H is small, N_2O can still be reduced through the reaction of $\text{N}_2\text{O} (+\text{M}) = \text{N}_2 + \text{O} (+\text{M})$. However, if the amount of H radical is insufficient and the stagnation wall temperature is low, then N_2O cannot be reduced through either of these two reactions. Thus, N_2O is detected in the products as a product gas.

Acknowledgments

The part of this study was supported by the Suzuki Foundation and the collaborative research project of

the Institute of Fluid Science, Tohoku University (Project code: J2111026).

Supplementary material

Detailed explanation of the mixture inlet velocity, the estimated stagnation wall temperature, and the polynomials used for the numerical simulation were provided in the supplementary material.

References

- [1] H. Kobayashi, A. Hayakawa, K.D.K.A. Somaratne, E.C. Okafor, Science and technology of ammonia combustion, *Proc. Combust. Inst.* 37 (2019) 109-133.
- [2] A. Valera-Medina, H. Xiao, M. Owen-Jones, W.I.F. David, P.J. Bowen, Ammonia for power, *Prog. Energy Combust. Sci.* 69 (2018) 63-102.
- [3] O. Kurata, N. Iki, T. Matsunuma, T. Inoue, T. Tsujimura, H. Furutani, H. Kobayashi, A. Hayakawa, Performances and emission characteristics of NH_3 -air and NH_3 - CH_4 -air combustion gas-turbine power generations, *Proc. Combust. Inst.* 36 (2017) 3351-3359.
- [4] M. Comotti, S. Frigo, Hydrogen generation system for ammonia-hydrogen fuelled internal combustion engines, *Int. J. Hydrogen Energy* 40 (2015) 10673-10686.
- [5] M. Koike, T. Suzuoki, T. Takeuchi, T. Homma, S. Hariu, Y. Takeuchi, Cold-start performance of an ammonia-fueled spark ignition engine with an on-board fuel reformer, *Int. J. Hydrogen Energy* 46 (2021) 25689-25698.
- [6] A.A. Khateeb, T.F. Guiberti, X. Zhu, M. Younes, A. Jamal, W.L. Roberts, Stability limits and NO emissions of technically-premixed ammonia-hydrogen-nitrogen-air swirl flames, *Int. J. Hydrogen Energy* 45 (2020) 22008-22018.
- [7] J.H. Lee, J.H. Kim, J.H. Park, O.C. Kwon, Studies on properties of laminar premixed hydrogen-added ammonia/air flames for hydrogen production, *Int. J. Hydrogen Energy* 35 (2010) 1054-1064.
- [8] A. Ichikawa, A. Hayakawa, Y. Kitagawa, K.D.K.A. Somaratne, T. Kudo, H. Kobayashi, Laminar burning velocity and Markstein length of ammonia/hydrogen/air premixed flames at elevated pressures, *Int. J. Hydrogen Energy* 40 (2015) 9570-9578.
- [9] G.J. Gotama, A. Hayakawa, E.C. Okafor, R. Kanoshima, M. Hayashi, T. Kudo, H. Kobayashi, Measurement of the laminar burning velocity and kinetics study of the importance of the hydrogen recovery mechanism of ammonia/hydrogen/air premixed flames, *Combust. Flame* 236 (2022) 11753.
- [10] C.B. Brackmann, V.A. Alekseev, B. Zhou, E. Nordström, P.-E. Bengtsson, Z. Li, M. Aldén, A.A. Konnov, Structure of premixed ammonia + air at atmospheric pressure: Laser diagnostics and kinetic modeling, *Combust. Flame* 163 (2016) 370-381.
- [11] A. Hayakawa, Y. Hirano, E.C. Okafor, H. Yamashita, T. Kudo, H. Kobayashi, Experimental and numerical study of product gas characteristics of ammonia/air premixed laminar flame stabilized in a stagnation flow, *Proc. Combust. Inst.* 38 (2021) 2409-2417.

- [12] K.D.K.A. Somarathne, S. Hatakeyama, A. Hayakawa, H. Kobayashi, Numerical study of a low emission gas turbine like combustor for turbulent ammonia/air premixed swirl flames with a secondary air injection at high pressure, *Int. J. Hydrogen Energy* 42 (2017) 27388-27399.
- [13] O. Kurata, N. Iki, T. Inoue, T. Matsunuma, T. Tsujimura, H. Furutani, M. Kawano, K. Arai, E.C. Okafor, A. Hayakawa, H. Kobayashi, Development of a wide range-operatable, rich-lean low-NO_x combustor for NH₃ fuel gas-turbine power generation, *Proc. Combust. Inst.* 37 (2019) 4587-4595.
- [14] S. Mashruk, M. Kovaleva, C.T. Chong, A. Hayakawa, E.C. Okafor, A. Valera-Medina, Nitrogen oxides as a by-product of ammonia/hydrogen combustion regimes, *Chem. Eng. Trans.* 89 (2021) 613-618.
- [15] United States Environmental Protection Agency, available at "<https://www.epa.gov/ghgemissions/understanding-global-warming-potentials>" (accessed on 2022 Jan. 3).
- [16] E.C. Okafor, M. Tsukamoto, A. Hayakawa, K.D.K.A. Somarathne, T. Kudo, T. Tsujimura, H. Kobayashi, Influence of wall heat loss on the emission characteristics of premixed ammonia-air swirling flames interacting with the combustor wall, *Proc. Combust. Inst.* 38 (2021) 5139-5146.
- [17] A. Hayakawa, Y. Hirano, A. Ichikawa, K. Matsuo, T. Kudo, H. Kobayashi, Novel dilution sampling method for gas analysis with a low sampling rate, *Mech. Eng. J.* 7 (2020) 19-00193.
- [18] ANSYS CHEMKIN-PRO 19.0, 2017
- [19] E.C. Okafor, Y. Naito, S. Colson, A. Ichikawa, T. Kudo, A. Hayakawa, H. Kobayashi, Experimental and numerical study of the laminar burning velocity of CH₄-NH₃-air premixed flames *Combust. Flame*, 187 (2018) 185-198.
- [20] H. Nakamura, S. Hasegawa, T. Tezuka, Kinetic modeling of ammonia/air weak flames in a micro flow reactor with a controlled temperature profile, *Combust. Flame* 185 (2017) 16-27.
- [21] H. Nakamura, S. Hasegawa, T. Tezuka, available from "<http://www.ifs.tohoku.ac.jp/enerdyn/en/result/mechanism.html>"
- [22] J. Otomo, M. Koshi, T. Mitsumori, H. Iwasaki, K. Yamada, Chemical kinetic modeling of ammonia oxidation with improved reaction mechanism for ammonia/air and ammonia/hydrogen/air combustion, *Int. J. Hydrogen Energy* 43 (2018) 3004-3014.
- [23] A. Stagni, C. Cavallotti, S. Arunthanayothin, Y. Song, O. Herbinet, F. Battin-Leclerc, T. Faravelli, An experimental, theoretical and kinetic-modeling study of the gas-phase oxidation of ammonia, *React. Chem. Eng.* 5 (2020) 696-711.
- [24] X. Zhang, S.P. Moosakutty, R. P. Rajan, M. Younes, S.M. Sarathy, Combustion chemistry of ammonia/hydrogen mixtures: Jet-stirred reactor measurements and comprehensive kinetic modeling, *Combust. Flame* 234 (2021) 111653.
- [25] J.A. Miller, C.T. Bowman, Mechanism and modeling of nitrogen chemistry in combustion, *Prog. Energy Combust. Sci.* 15 (1989) 287-338.